# Separating Feeder Demand Into Components Using Substation, Feeder, and Smart Meter Measurements

Gregory S. Ledva, *Member, IEEE*, and Johanna L. Mathieu, *Senior Member, IEEE*

***Abstract*—Real-time, feeder-level energy disaggregation seeks to separate the measured total demand of a distribution feeder into components (e.g., into the aggregate demand-responsive load and remaining demand on the feeder, or into the aggregate generation and demand on the feeder). It can benefit distribution system operators and demand response providers by providing real-time information about balancing reserve requirements or the aggregate demand-responsive load, among other applications. In this work, we develop a feeder-level energy disaggregation algorithm that uses measurements from multiple sources that are available on different timescales. The algorithm is based on online learning and uses sensor fusion to incorporate output equations associated with disparate active and reactive power flow measurements, complex bus voltage measurements, and residential smart meter measurements. The algorithm also uses distribution substation measurements. Case studies simulate a three-phase distribution feeder model with unbalanced loads, where the active and reactive demand of the loads are modeled as a function of voltage and temperature. These models are parameterized using real-world active power demand data at each time-step. Results indicate that disaggregating three demand components is possible using feeder head active power measurements, that including feeder head reactive power measurements improves disaggregation accuracy by 32% on average, and that including intermittent real-time smart meter measurements further improves disaggregation accuracy.**

***Index Terms*—Distribution system, energy disaggregation, power flow, smart meters.**

## I. Introduction

DISTRIBUTED energy resources (DERs) such as residential solar installations and residential demand responsive loads are becoming more prevalent within distribution networks [1], [2]. These technologies can cause more variability in distribution network power flows, requiring additional sensing to maintain acceptable power quality to end-users. Real-time sensing in distribution networks has traditionally been limited to within the substations [3]. However, additional real-time sensing capabilities outside of the substation, e.g., of bus voltage phasors, are becoming more common [4]. Smart meters have also been widely deployed [2], and they can provide device-level power usage information via energy disaggregation algorithms [5], but smart meter communication capabilities limit the real-time availability of these measurements. The information commonly is transmitted only once per hour, or once per day.

In this work, we use real-time and historical measurements from a distribution substation, a distribution feeder, and smart meters to perform real-time, feeder-level energy disaggregation on time-scales of seconds to minutes. Real-time, feeder-level energy disaggregation seeks to separate the measured total demand of a distribution feeder into components. Examples of possible demand/generation components include the aggregate demand-responsive load and the remaining demand on the feeder, the aggregate generation and the demand on the feeder, or the aggregate voltage-dependent load and the remaining load. It can benefit distribution system operators and demand response providers by providing information about 1) potential balancing reserve requirements due to changes in solar generation, 2) the real-time aggregate demand of the demand-responsive loads which can be used as a feedback signal for control algorithms, and 3) the potential benefits of conservation voltage reduction, among other applications. For example, [6] uses disaggregation to determine the load on a feeder that also has substantial solar generation. Works [7], [8] assume a feedback signal (i.e., the aggregate demand of a collection of demand-responsive loads) is available for real-time control.

In this work, we develop a feeder-level energy disaggregation algorithm using an online learning algorithm that we modify to incorporate sensor fusion, which is a method to utilize data/information from disparate sources/sensors within an estimate, e.g., see [9]. Sensor fusion allows the algorithm to utilize real-time measurements that are available on different timescales from a variety of sources. We use historical measurements to compute demand component models that predict the real-time demand of the components, and we adjust these predictions using real-time measurements. Case studies disaggregate the real-time feeder demand into the aggregate air conditioner (AC) demand, the aggregate demand of non-air conditioning loads, referred to as the other load (OL) demand, and the network (NW) demand, i.e., the losses and capacitor bank reactive power injections.

Related feeder-level energy disaggregation literature includes the following: [6] uses multiple linear regression with substation apparent power measurements; [10] and [11] use artificial neural networks with substation apparent power (in some cases, only active power) and

Manuscript received July 11, 2019; revised November 25, 2019; accepted January 13, 2020. Date of publication January 17, 2020; date of current version June 19, 2020. This work was supported by NSF under Grant ECCS-1508943 and Grant CNS-1837680. Paper no. TSG-00983-2019. *(Corresponding author: Gregory S. Ledva.)*

The authors are with the Department of Electrical Engineering and Computer Science, University of Michigan, Ann Arbor, MI 48109 USA (e-mail: gsledv@umich.edu; jlmath@umich.edu).

Color versions of one or more of the figures in this article are available online at http://ieeexplore.ieee.org.

Digital Object Identifier 10.1109/TSG.2020.2967220

voltage measurements; [12] estimates the load based on assumed models of the load components using substation apparent power and voltage measurements; and our prior work [13], [14] use online learning and substation active power measurements.

The contributions of this work are the following: 1) we formulate a more general disaggregation problem that includes the reactive power and the NW demand making the algorithm more applicable to real power systems, whereas [13], [14] include only the active demand and no NW demand; 2) we develop the non-trivial ability to include additional real-time heterogeneous measurements from the feeder outside of the substation and from smart meters, and we incorporate measurements taken on different time-scales, both of which greatly enhance the flexibility of the algorithm, whereas [6], [10]–[14] only use real-time measurements from the substation on the same time-scales; 3) in the case studies we explicitly model the distribution feeder, the resulting NW demand, and the feeder's influence on the measured aggregate power of the feeder, whereas [6], [10]–[14] do not; 4) we generate case study data using real-world active power data and realistic models to generate reactive power data, voltage dependence, and outdoor temperature dependence, whereas [10]–[12] all use artificial training and testing data; and 5) we investigate changes in disaggregation accuracy when including reactive power, voltage phasors, and complex current (into aggregate models), which helps inform whether additional sensing capabilities on a given feeder might be beneficial or cost-effective, whereas [10] investigates reactive power only. Contribution 2) allows the algorithm to leverage the diverse sensors that may exist on real radial feeders, which often have more than just feeder head power flow measurements available. We emphasize that using heterogeneous measurements such as power flows and voltage phasors to disaggregate load requires substantial non-trivial modifications for the formulations in the literature; that is the focus of this work.

The remainder of the work is organized as follows: Section II describes the problem overview; Section III details the energy disaggregation algorithm; Section IV describes the aggregate modeling in the disaggregation algorithm; Section V details the case studies; and Section VI concludes.

## II. Problem Overview

A power system entity, e.g., a demand response provider or distribution system operator, seeks to estimate the real-time aggregate demand of $N$ demand components served by a distribution feeder on timescales of seconds to minutes via feeder-level energy disaggregation. Figure 1 illustrates an example of feeder-level energy disaggregation. The entity measures the demand of (i.e., the power flow into) a distribution feeder and estimates the feeder's aggregate AC, OL, and NW demands.

Fig. 2 summarizes the plant (i.e., the physical system of interest), the disaggregation algorithm, and possible real-time measurements. The plant contains a distribution substation, a distribution feeder, and residences, which contain loads that

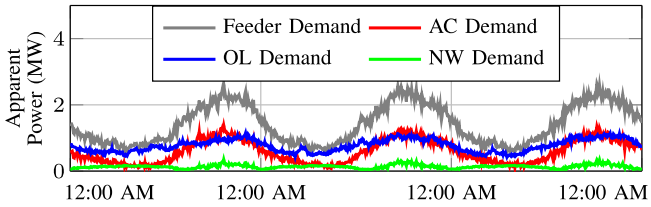


Fig. 1. Time series of the feeder demand and the demand components.

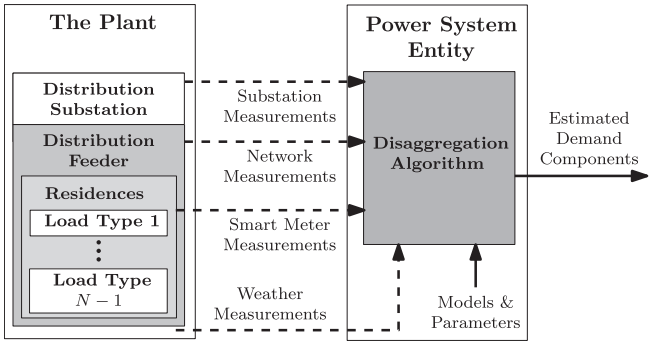


Fig. 2. Block diagram depicting the main components within the problem framework and the potential real-time measurements.

TABLE I
Possible Real-Time Measurements

| Measurement Type | Frequency |
|---|---|
| Substation Measurements | |
| Active and reactive power flow into the feeder | 1 minute |
| Complex current flowing into the feeder | 1 minute |
| Complex voltage at the feeder head | 1 minute |
| Network Measurements | |
| Active and reactive power flow within the feeder | 1 minute |
| Complex voltage within the feeder | 1 minute |
| Smart Meter Measurements | |
| Active and reactive power flowing into the residence | 10-60 minutes |
| Current magnitude flowing into the residence | 10-60 minutes |
| Voltage magnitude at the residence | 10-60 minutes |
| Voltage and current phase difference at the residence | 10-60 minutes |
| Weather Measurements | |
| Outdoor temperature | 1 minute |

can be separated into $N-1$ components. The $N$th demand component is the NW demand.

We assume that the power system entity receives some combination of substation, network, smart meter, and weather measurements in real-time. Table I illustrates possible measurements and their assumed frequency of availability for the case studies of Section V. We assume that 1) substation measurements are available as substations are extensively metered [3]; 2) network measurements, i.e., measurements at points within the distribution feeder outside of the substation, may be available from sensors such as micro-phasor measurement units [4]; 3) smart meter measurements may be available but only at infrequent intervals, e.g., every 10-60 minutes, due to smart meter communication limitations [5]; and 4) weather measurements are available from weather sensors near the feeder.

We also assume that when smart meter measurements are available from all residences we can directly compute

the $N$ demand components for the feeder by 1) applying building-level energy disaggregation algorithms [5] to each meter's measurements, 2) summing the demands of the loads that correspond to each demand component, and 3) computing the NW demand by subtracting the total demand measured by the smart meters from the measured feeder demand. The smart meter capabilities enabling this include their ability 1) to measure apparent power, voltage and current magnitudes, and the phase difference between the voltage and current; 2) to sample measurements on timescales of seconds to minutes; and 3) to transmit histories of measurements [5]. We also assume that historical smart meter measurements are always available on timescales of seconds to minutes, regardless of whether they are transmitted in real-time.

The feeder-level energy disaggregation algorithm computes demand component estimates for the total feeder, measured at the distribution substation (i.e., at the feeder head). The algorithm computes demand component estimates for the present time-step by updating demand component estimates for the previous time-step using the real-time measurements, sensor fusion, and aggregate models (and their parameters). First, we fuse the available real-time substation, network, and smart meter measurements, where the modeling approach for the measurements relies on a radial feeder structure. Next, we compute measurement-based prediction adjustments using the fused measurements and the demand component estimates for the previous time-step. Then, we compute the model-based predictions using the aggregate models, weather measurements, and (possibly) substation measurements. Finally, we estimate the demand components at the next time-step using the new predictions and the prediction adjustment. While the goal is disaggregation of the total demand at the feeder head, the demand components are split over portions of the feeder to facilitate the usage of network measurements outside of the substation.

The case-study plant includes a three-phase distribution feeder model with unbalanced, wye-connected (line-to-neutral) loads. However, the aggregate models and the disaggregation algorithm do not model coupling between the phases; they model and disaggregate each phase individually and implicitly assume wye-connected loads. Therefore, for simplicity, we exclude notation specifying the phase. This implicit assumption is mild as delta-connected loads are relatively rare on distribution systems in the United States. Extension to systems with delta-connected loads is a subject for future research.

## III. The Energy Disaggregation Algorithm

The feeder-level energy disaggregation algorithm consists of an estimation algorithm, sensor fusion methodology, and output equations for distribution system measurements. The estimation algorithm incorporates these output equations via the sensor fusion methodology, which allows the disaggregation algorithm to use measurements from multiple sources that are available on different timescales. Section III-A summarizes a previously developed estimation algorithm. Section III-B summarizes the sensor fusion methodology, which builds on the prior subsection to show how multiple measurement sources can be utilized within the algorithm. Section III-C develops output equations for four measurement types within the distribution system: power flows, squared bus voltage magnitude differences, bus voltage angle differences, and smart meter measurements. This subsection builds on the prior ones by detailing the specific output equations for the various measurements, which can then all be utilized in the estimation algorithm via the sensor fusion methodology.

### A. The Estimation Algorithm

The estimation algorithm is a modified version of Dynamic Mirror Descent (DMD), an online learning algorithm developed in [15] and modified in [13]. DMD iterates between a measurement-based update and a model-based update. The measurement-based update computes an adjusted state estimate via a convex optimization formulation that incorporates newly arrived measurements. The model-based update advances the adjusted state estimate to the next time-step via a possibly nonlinear model. Reference [13] modified DMD to separate the measurement-based update from the model-based update, allowing the use of a wider range of models within the algorithm.

The modified DMD algorithm computes estimates $\widehat{\theta}_t \in \Theta$ of a dynamic state $\theta_t \in \Theta$ using measurements $y_t \in \mathcal{Y}$ that arrive sequentially in time. The domain of the state $\Theta \subset \mathbb{R}^{d_1}$ is a bounded, closed, convex feasible set of dimension $d_1$, and $\mathcal{Y} \subset \mathbb{R}^{d_2}$ is the domain of the measurements with dimension $d_2$. For feeder-level energy disaggregation, $\theta_t$ is a vector of aggregate demand components for different types of loads or generation, possibly aggregated over separate portions of a distribution feeder. Modified DMD is as follows

$$\widehat{\kappa}_{t+1} = \operatorname*{arg\,min}_{\theta \in \Theta} \left[ \eta^{\mathrm{s}} \left\langle \nabla \ell_t \left( \widehat{\theta}_t, y_t \right), \ \theta \right\rangle + D(\theta \| \widehat{\kappa}_t) \right] \quad (1)$$

$$\breve{\theta}_{t+1} = \Phi \left( \breve{\theta}_t \right) \quad (2)$$

$$\widehat{\theta}_{t+1} = \breve{\theta}_{t+1} + \widehat{\kappa}_{t+1}, \quad (3)$$

where $\widehat{\kappa}_t$ accumulates the measurement-based adjustment to $\widehat{\theta}_t$, and $\breve{\theta}_t$ is the model-based prediction. Eq. (1) updates $\widehat{\kappa}_t$ to include the new measurement, where the first term penalizes deviations of the model predictions from the measurements, where the second term penalizes the accumulation of errors, and where $\eta^{\mathrm{s}}$ controls the trade-off between the terms. Eq. (2) predicts the state at the next time-step using the model $\Phi(\cdot)$, and (3) adjusts the model-based prediction using $\widehat{\kappa}_t$. In the above, $\eta^{\mathrm{s}} \in (0, 1]$ is a user-defined step-size parameter, $\langle \cdot, \ \cdot \rangle$ is the standard dot product, $\nabla \ell_t(\cdot, y_t)$ is a gradient or subgradient of the user-defined loss function $\ell_t(\cdot, y_t)$ that penalizes deviations of the predicted measurement from $y_t$ with $y_t$ fixed, $\theta$ is the optimization variable, and $D(\cdot \| \cdot)$ is a user-defined Bregman divergence that is a measure of distance between the arguments. We assume that $\ell_t(\widehat{\theta}_t, y_t)$ contains a linear mapping from $\widehat{\theta}_t$ to the estimated output $\widehat{y}_t$, i.e., that $\widehat{y}_t = C_t \widehat{\theta}_t$, where the matrix $C_t$ depends on the available measurements at each time-step. We also assume that $\ell_t(\widehat{\theta}_t, y_t)$ contains an output estimation error covariance matrix $\Pi_t^{\mathrm{y}}$, i.e., a covariance matrix that quantifies the accuracy of the output estimates, as this can improve disaggregation accuracy [14].

The models $\Phi(\cdot)$ can come from an arbitrary source (e.g., operator experience or data), can have arbitrary structure (e.g., state-space or regression models), and may be inaccurate at times. Reference [13] used $\breve{\theta}_t$ as the argument of $\Phi(\cdot)$ to allow usage of models of with different structures, and [13] and [14] both utilize an extension of DMD from [15] that uses multiple $\Phi(\cdot)$ sets to address modeling inaccuracy. The algorithmic developments in this work, [13], and [14] can be incorporated into an energy disaggregation algorithm simultaneously to address modeling error and heterogeneous measurements.

### B. Sensor Fusion Methodology

We summarize a sensor fusion methodology to construct $C_t$ within modified DMD based on the newly available real-time measurements at time $t$. Kalman filtering commonly uses sensor fusion [9], but feeder-level energy disaggregation has not used it. We assume the output equation of each measurement is

$$y_t = C_t\theta_t + w_t, \tag{4}$$

where $w_t$ is the measurement noise, which we assume is a random vector with positive-definite measurement error covariance $R$. Given two measurements $y_t^1$, $y_t^2$, their respective output matrices $C_t^1$, $C_t^2$, and their respective measurement error covariances $R^1$, $R^2$, we assume that the measurement noise for separate sensors are independent, and the fused output quantities are

$$\begin{bmatrix}\widehat{y}_t^1\\ \widehat{y}_t^2\end{bmatrix} = \begin{bmatrix}C_t^1\\ C_t^2\end{bmatrix}\widehat{\theta}_t \text{ with } R = \begin{bmatrix}R^1 & 0\\ 0 & R^2\end{bmatrix}. \tag{5}$$

We assume that the estimation errors are independent of each other and from the measurement noise and compute $\Pi_t^{\mathrm{y}} = C_t\widehat{\Pi}_t C_t^{\mathrm{T}} + R$, where $\widehat{\Pi}_t$ is the state estimation error covariance.

The sensor fusion methodology allows measurements on different timescales to be utilized within the algorithm. For example, if power flow measurements are available at all time-steps and smart meter measurements are available intermittently, a fused output equation and measurement noise covariance can be computed for time-steps when both measurements are available, and the power flow measurements can be used within the algorithm for the remaining time-steps.

### C. Output Equations

This subsection develops feeder-level energy disaggregation output equations for the four measurement types. We first introduce notation and then define the output matrix and measurement error covariance for each measurement type. Feeder-level energy disaggregation seeks to separate the total feeder demand, measured at the feeder head, into different demand components aggregated over the entire feeder. Some measurements (e.g., power flows) may provide information about portions of the feeder (e.g., the downstream demand). As a result, we extend the common feeder notation to describe feeder portions, rather than describing individual feeder nodes, allowing us to incorporate these measurements. If measurements are only available at the substation or feeder head, then this is unnecessary, and the algorithm should be formulated for the entire feeder. We represent power flows on a radial feeder as sums of the downstream load and losses, and so the output matrices are only valid for radial feeders. To simplify notation, we exclude time indices in this subsection; however, the approach could accommodate time-varying sets and parameters, if they and their evolution are known.

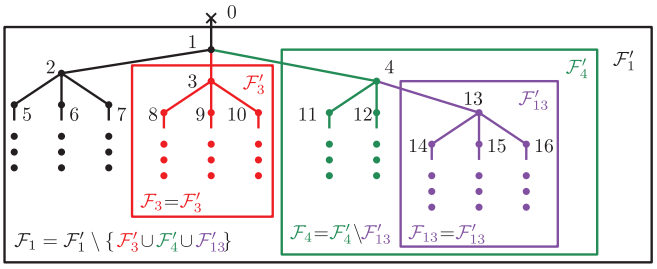


Fig. 3. Example feeder and feeder portions $\mathcal{F}_m'$ (within boxes) and $\mathcal{F}_m$ (differentiated by color) for $m \in \mathcal{M} = \{1, 3, 4, 13\}$. Vertical ellipses indicate an arbitrary downstream feeder structure. Node 0 is the root, indicated with a cross.

We first describe the feeder as a graph consisting of a set of buses/nodes $\mathcal{N}$ and a set of power lines/edges $\mathcal{E}$ connecting the nodes in a radial/rooted-tree topology. In a radial/tree topology, 1) all nodes within the graph are reachable from any other node via a path, or a sequence of nodes and edges, and 2) no path exists from a node back to itself using unique edges. In a rooted tree, one node is the root (a node within the substation in this case), and a parent-child designation exists between the nodes $m$ and $n$ connected via an edge $(m, n) \in \mathcal{E}$. The parent is $m$ (i.e., the upstream node, or the node closer to the root), and $n$ is the child (i.e., the downstream node). The root has no parent, every other node has one parent, and nodes can have multiple/no child nodes. The descendants of node $n$ are the nodes downstream of $n$ (i.e., the nodes that contain $n$ on the path from the node of interest to the root).

If the feeder topology is known/estimated, we can define portions of the feeder $\mathcal{F}_m$ for $m \in \mathcal{M}$ as subsets of edges and nodes. The set $\mathcal{M}$ is known, and it consists of $M$ nodes of interest, where the nodes are either measurement points or nodes between bus voltage magnitude/angle measurement points. Sections III-C1–III-C4 detail the addition of nodes into $\mathcal{M}$ based on the available measurements of each type. Knowledge of the feeder topology equates to knowledge of the adjacency matrix, which indicates the children of each node. The distribution system operator could disclose the feeder topology, or it could be estimated, e.g., using voltage magnitude measurements from smart meters [16].

Given $\mathcal{M}$, we first define preliminary feeder portions as $\mathcal{F}_m' = \{\mathcal{N}_m, \mathcal{E}_m\}$ for $m \in \mathcal{M}$, where the set $\mathcal{N}_m$ consists of node $m$ plus its descendants and $\mathcal{E}_m$ is the set of edges downstream from $m$ plus the edge connecting $m$ to its parent node. Then, to ensure that the feeder portions have no nodes/edges in common, we remove any preliminary feeder portions that are downstream from $\mathcal{F}_m'$, i.e., $\mathcal{F}_m = \mathcal{F}_m' \backslash \{\cup_{n\in\mathcal{D}^m}\mathcal{F}_n'\}$, where $\cdot\backslash\cdot$ is the set minus operator, $\cup$ is the set union operator, and $\mathcal{D}^m$ contains any elements of $\mathcal{M}$ that are descendants of $m$.

**Example:** Figure 3 depicts an example feeder and forms $\mathcal{F}_m'$ and $\mathcal{F}_m$ for $\mathcal{M} = \{1, 3, 4, 13\}$. The boxes each contain an $\mathcal{F}_m'$, and the node/edge color indicates the corresponding $\mathcal{F}_m$.

For nodes 3 and 13, $\mathcal{F}_3 = \mathcal{F}'_3$ and $\mathcal{F}_{13} = \mathcal{F}'_{13}$ as there are no downstream nodes within $\mathcal{M}$. Node 13 is downstream of node 4, and so $\mathcal{F}_4 = \mathcal{F}'_4 \backslash \mathcal{F}'_{13}$. Nodes 3, 4, and 13 are all downstream of node 1, and so $\mathcal{F}_1 = \mathcal{F}'_1 \backslash \{\mathcal{F}'_3 \cup \mathcal{F}'_4 \cup \mathcal{F}'_{13}\}$. Node 0 is the root, indicated with a cross, and is excluded from feeder portions as it is unused in the calculations for each measurement type.

We now introduce the state vector $\theta$ and the general output equation. For feeder-level energy disaggregation, $\theta$ consists of the active and reactive power consumption of the $N$ demand components for the feeder portions $\mathcal{F}_m \in \mathcal{M}$:

$$\theta \triangleq \left[P^{\mathrm{T}}_{\mathcal{F}_{m_1}} \cdots P^{\mathrm{T}}_{\mathcal{F}_{m_M}} Q^{\mathrm{T}}_{\mathcal{F}_{m_1}} \cdots Q^{\mathrm{T}}_{\mathcal{F}_{m_M}}\right]^{\mathrm{T}}, \tag{6}$$

where $m_1, \ldots, m_M$ are the elements of $\mathcal{M}$, and where $(\cdot)^{\mathrm{T}}$ denotes the transpose. The elements of $P_{\mathcal{F}_m} \in \mathbb{R}^N$ and $Q_{\mathcal{F}_m} \in \mathbb{R}^N$ are the active and reactive power consumption of the $N$ demand components aggregated over $\mathcal{F}_m$, which is detailed in Section III-C1. The general output equation is

$$y = C\theta = \left[c^N_{m_1} \cdots c^N_{m_M} \, d^N_{m_1} \cdots d^N_{m_M}\right]\theta, \tag{7}$$

where $c^N_m$, $d^N_m$ for $m \in \mathcal{M}$ are $N$-element row vectors.

*1) Active and Reactive Power Flow Measurements:* Next, we develop output equations for measurements of the active and reactive power flow out of a node. We do this by manipulating the DistFlow equations from [17] into sums of the $N$ demand components over feeder portions, i.e., into sums over elements of $\theta$. Reference [18] approximates the power flows as sums of the net load (i.e., demand minus generation) at the downstream nodes; we extend this to include active and reactive losses.

The reactive power flow $Q_{m,n}$ out of node $m$ towards $n$ is

$$Q_{m,n} = \sum_{k:(n,k)\in\mathcal{E}} Q_{n,k} + \sum_{l=1}^{N-1} Q^l_n + Q^{\mathrm{cap}}_n + x_{m,n} i^2_{m,n} \tag{8}$$

where $Q^l_k$ is the reactive power consumption of demand component $l$ at node $k$, $Q^{\mathrm{cap}}_k$ is the capacitor bank power injection at node $k$, $x_{m,n}$ is the reactance of edge $(m,n)$, and $i^2_{m,n}$ is the squared current magnitude on edge $(m,n)$. In (8), the first term computes the power flows out of node $n$, the second and third terms compute the reactive power consumption at node $n$, and the last term computes the reactive losses on $(m,n)$. We now manipulate (8) into the form of (7):

$$\begin{aligned} Q_{m,n} &= \sum_{k\in\mathcal{N}_n} \sum_{l=1}^{N-1} Q^l_k + \sum_{k\in\mathcal{N}_n} Q^{\mathrm{cap}}_k + \sum_{(g,h)\in\mathcal{E}_n} x_{g,h} i^2_{g,h} \qquad (9) \\ &= \sum_{k\in\{\mathcal{D}^n \cup n\}} \mathbf{1}^{\mathrm{T}} Q_{\mathcal{F}_k}, \qquad (10) \end{aligned}$$

where $\mathbf{1}$ is a column-vector of ones. In (9), we reformulate $Q_{m,n}$ into sums over sets of nodes and edges. In (10), we reformulate $Q_{m,n}$ into sums of the $N$ demand components within $Q_{\mathcal{F}_k}$ for $k \in \{\mathcal{D}^n \cup n\}$, i.e., over the feeder portions needed to form the sets $\mathcal{N}_n$ and $\mathcal{E}_n$. Specifically, we compute the elements of $Q_{\mathcal{F}_m}$ for the $N-1$ load types as $Q^l_{\mathcal{F}_m} = \sum_{k\in\mathcal{N}(\mathcal{F}_m)} Q^l_k$ for $l = 1, \ldots, N-1$, where $\mathcal{N}(\mathcal{F}_m)$ is the set of nodes in the feeder portion. We compute the element of $Q_{\mathcal{F}_m}$ corresponding to the reactive NW demand as $Q^N_{\mathcal{F}_m} = \sum_{k\in\mathcal{N}(\mathcal{F}_m)} Q^{\mathrm{cap}}_k + \sum_{(g,h)\in\mathcal{E}(\mathcal{F}_m)} x_{g,h} i^2_{g,h}$, where $\mathcal{E}(\mathcal{F}_m)$ is the set of edges in the feeder portion. We compute an active power flow $P_{m,n}$ using equations similar to (8)–(10) without the capacitor bank term and replacing $x_{m,n}$ with resistance $r_{m,n}$. We include in $\mathcal{M}$ the downstream node of any power flow measurement, e.g., $n$ for $Q_{m,n}$.

**Example (continued):** To illustrate (10), we continue the example in Fig. 3. Assume that we have $P_{0,1}$, $Q_{0,1}$, $P_{1,3}$, and $Q_{1,3}$ measurements from $(0,1)$ and $(1,3)$. Therefore, nodes 1 and 3 are included in $\mathcal{M}$. Assume nodes 4 and 13 are also included in $\mathcal{M}$ because they correspond to other measurements, discussed in the next sections. According to (9), $P_{0,1}$ ($Q_{0,1}$) is the sum of the active (reactive) power consumption at all non-root nodes in the feeder and the active (reactive) losses along all lines. According to (10), $\{\mathcal{D}^1 \cup 1\} = \{\{3, 4, 13\} \cup 1\} = \{1, 3, 4, 13\}$, and we compute $P_{0,1}$ ($Q_{0,1}$) as the sum of the $N$ active (reactive) demand components aggregated over each feeder portion in $\{\mathcal{F}_1, \mathcal{F}_3, \mathcal{F}_4, \mathcal{F}_{13}\}$. Node 3 has no downstream nodes in $\mathcal{M}$, and so $\{\mathcal{D}^3 \cup 3\} = \{3\}$, and we compute $P_{1,3}$ and $Q_{1,3}$ using $\mathcal{F}_3$ only.

Equation (10) is the output equation for reactive power flows. To put it in the desired form (7), we set $c^N_k = \mathbf{0}^{\mathrm{T}}$ for all $k$ and $d^N_k = \mathbf{1}^{\mathrm{T}}$ for $k \in \{\mathcal{D}^n \cup n\}$, where $\mathbf{0}$ is a column-vector of zeros. For active power flows, $c^N_k = \mathbf{1}^{\mathrm{T}}$ for $k \in \{\mathcal{D}^n \cup n\}$ and $d^N_k = \mathbf{0}^{\mathrm{T}}$ for all $k$. We assume that power flow measurements are accurate, and so the corresponding measurement noise covariance is $R^{\mathrm{PQ}} \approx 0$. In cases with inaccurate power flow measurements, we can handle measurement noise by increasing $R^{\mathrm{PQ}}$, which is accounted for in the measurement-based update of DMD.

*2) Squared Voltage Magnitude Difference Measurements:* We now develop an output equation for measurements of the difference in squared voltage magnitude between two nodes along a path. We first summarize the linear Distflow equation approximating the difference in squared voltage magnitudes for two nodes connected via an edge then via a path. The approximation of this difference over an edge $(m,n)$ is [17]

$$V^2_{m,n} \approx 2(r_{m,n} P_{m,n} + x_{m,n} Q_{m,n}), \tag{11}$$

where $V^2_{m,n} = v^2_m - v^2_n$, and where $v^2_m$ is the squared voltage magnitude at node $m$. For a path from node $f$ to $s$ consisting of nodes $\mathcal{M}^{\mathrm{VM}}$ and edges $\mathcal{E}^{\mathrm{VM}}$, $V^2_{f,s}$ sums (11) over each edge in $\mathcal{E}^{\mathrm{VM}}$ [18]:

$$V^2_{f,s} = \sum_{(m,n)\in\mathcal{E}^{\mathrm{VM}}} (2r_{m,n} P_{m,n} + 2x_{m,n} Q_{m,n}). \tag{12}$$

In [18], $P_{m,n}$ and $Q_{m,n}$ are computed from the net loads at each node, ignoring losses. Here we include the losses, allowing us to capture the impact of losses on the squared voltage magnitude difference.

We include the nodes from $\mathcal{M}^{\mathrm{VM}}$ that appear as child nodes within $\mathcal{E}^{\mathrm{VM}}$ in $\mathcal{M}$ and reformulate (12) into sums over

elements of $\theta$:

$$V_{f,s}^2 = \sum_{(m,n)\in\mathcal{E}^{\mathrm{VM}}} \left( 2r_{m,n} \sum_{k\in(\mathcal{D}^n\bigcup n)} \mathbf{1}^{\mathrm{T}} P_{\mathcal{F}_k} + 2x_{m,n} \sum_{k\in(\mathcal{D}^n\bigcup n)} \mathbf{1}^{\mathrm{T}} Q_{\mathcal{F}_k} \right) \quad (13)$$

$$= \sum_{m\in\mathcal{M}} \left( \sum_{(g,h)\in\mathcal{U}^m} \left(2r_{(g,h)}\right) \mathbf{1}^{\mathrm{T}} P_{\mathcal{F}_m} + \sum_{(g,h)\in\mathcal{U}^m} \left(2x_{(g,h)}\right) \mathbf{1}^{\mathrm{T}} Q_{\mathcal{F}_m} \right), \quad (14)$$

where $\mathcal{U}^m$ is the set of edges upstream from node $m$ within $\mathcal{E}^{\mathrm{VM}}$. In (13), we use (10) and its active power analog to express the power flows as sums of the demand components over feeder portions. In (14), we rearrange the sums to collect the resistances and reactances for each feeder portion.

---

**Example (continued):** To illustrate (12)–(14), we continue the example using Fig. 3. Assume we have a measurement $V_{0,4}^2$, with $\mathcal{M}^{\mathrm{VM}} = \{0, 1, 4\}$ and $\mathcal{E}^{\mathrm{VM}} = \{(0, 1), (1, 4)\}$. Therefore, we need to include nodes 1 and 4 in $\mathcal{M}$, which already contains nodes 1 and 3 (from power flow measurements). Assume $\mathcal{M}$ also includes 13 (which corresponds to another measurement, discussed in the next section). Using (12), $V_{0,4}^2 = (2r_{0,1}P_{0,1} + 2x_{0,1}Q_{0,1}) + (2r_{1,4}P_{1,4} + 2x_{1,4}Q_{1,4})$. Using (13), $P_{0,1} = \mathbf{1}^{\mathrm{T}}(P_{\mathcal{F}_1}+P_{\mathcal{F}_3}+P_{\mathcal{F}_4}+P_{\mathcal{F}_{13}})$, and similarly for the other power flows; $\mathbf{1}^{\mathrm{T}}$ sums the demand components to compute the total demand measured at the substation/feeder head. In (14), $\mathcal{U}^4 = \mathcal{U}^{13} = \{(0, 1), (1, 4)\}$ and $\mathcal{U}^1 = \mathcal{U}^3 = \{(0, 1)\}$, and so (14) sums the resistance and reactance of lines $(0, 1)$ and $(1, 4)$ for $m = \{4, 13\}$ and sums the resistance and reactance of $(0, 1)$ for $m = \{1, 3\}$.

---

Finally, we put (14) into the desired form (7) by setting $c_m^{\mathrm{N}} = \sum_{(g,h)\in\mathcal{U}^m}(2r_{(g,h)})\mathbf{1}^{\mathrm{T}}$ and $d_m^{\mathrm{N}} = \sum_{(g,h)\in\mathcal{U}^m}(2x_{(g,h)})\mathbf{1}^{\mathrm{T}}$ for $m \in \mathcal{M}$. If we only have knowledge of the feeder topology, not the resistances and reactances, we can estimate the parameters in the output matrix using multiple linear regression on historical values of $V_{f,s}^2$ and estimates of $\theta$, where estimates of $\theta$ are detailed in Section III-C4. We compute $R^{\mathrm{VM}}$ as the covariance of the errors between the historical $V_{f,s}^2$ measurements and the predicted values using the parameterized output matrix. Measurement noise arises from the approximations used in (11), and from errors in estimating the output matrix and $\theta$.

*3) Voltage Angle Difference Measurements:* Here we develop an output equation for measurements of the difference in voltage angles between two nodes along a path containing nodes $\mathcal{M}^{\mathrm{VA}}$ and edges $\mathcal{E}^{\mathrm{VA}}$. Similar to the previous subsection, we add the nodes from $\mathcal{M}^{\mathrm{VA}}$ that appear as child nodes within $\mathcal{E}^{\mathrm{VA}}$ into $\mathcal{M}$. From [18], the linear equation approximating $\delta_{m,n}$ across edge $(m, n)$, is

$$\delta_{m,n} \approx x_{m,n}P_{m,n} - r_{m,n}Q_{m,n}. \quad (15)$$

This is similar to (11), where the resistance and reactance are swapped, the resistance is made negative, and the right-hand side is scaled by 0.5. The voltage angle difference equation for a path has the same form as (14), where the sums of resistances and reactances are swapped and scaled by 0.5, the resistances are made negative, and the set $\mathcal{U}^m$ contains the upstream edges in $\mathcal{E}^{\mathrm{VM}}$. To put the voltage angle analog of (14) into the desired form (7), we either set $d_m^{\mathrm{N}} = \sum_{(g,h)\in\mathcal{U}^m}(-r_{(g,h)})$ and $c_m^{\mathrm{N}} = \sum_{(g,h)\in\mathcal{U}^m}(x_{(g,h)})$ for $m \in \mathcal{M}$ or use the matrix parameters identified in Section III-C2 while swapping, scaling, and making them negative as detailed above.

---

**Example (continued):** To illustrate the voltage angle analog of (14), we continue the example using Fig. 3. Assume we have measurement $\delta_{0,13}$ with $\mathcal{M}^{\mathrm{VA}} = \{0, 1, 4, 13\}$ and $\mathcal{E}^{\mathrm{VA}} = \{(0, 1), (1, 4), (4, 13)\}$. Therefore, we need to include nodes 1, 4, and 13 into $\mathcal{M}$, which already contains nodes 1, 3, and 4 from previous measurements. The resistance/reactance sums for $P_{\mathcal{F}_m}$ and $Q_{\mathcal{F}_m}$ with $m \in \mathcal{M}$ were identified for (14). Therefore, we 1) scale all identified parameters by 0.5, 2) swap the identified parameters corresponding to sums of resistances with those corresponding to sums of reactances, and 3) make negative the parameters corresponding to sums of resistances.

---

We compute $R^{\mathrm{VA}}$, the measurement noise covariance for voltage angle measurements, using the historical accuracy of the measured angle difference versus the predicted angle difference given historical estimates of $\theta$ (detailed in Section III-C4), and the corresponding output matrix. The measurement noise arises from approximations used in (15) and from errors in estimating $\theta$ and the parameters in $C$.

*4) Smart Meter Measurements:* Here we develop an output equation for real-time smart meter active and reactive power measurements. The smart meter measurements do not affect $M$ and $\theta$. As described in Section II, during time-steps when smart meter measurements are available in real-time, we assume that we can compute estimates of the $N$ demand components for the entire feeder using building-level energy disaggregation. Furthermore, we can estimate the $N$ demand components for portions of the feeder, i.e., for elements in $\theta$. Assuming we do not have measurements of NW demand in each feeder portion, we can approximate the NW demand in each feeder portion by scaling the total feeder NW demand using the number of edges within the feeder portion. For example, $P_{\mathcal{F}_{13}}^{\mathrm{N}} = P^N|\mathcal{E}(\mathcal{F}_{13})|(|\mathcal{E}|)^{-1}$ where $P^N$ is the total NW demand of the feeder, and where $|\cdot|$ is used to denote the cardinality of the argument set. Therefore, the output equation in the form (7) is

$$y = \left[I\right]\theta, \quad (16)$$

where $I$ is an appropriately-sized identity matrix. We assume that any inaccuracies in disaggregating the smart meter data at the household level are negligible when summing the disaggregated demand components across houses to compute the feeder-level measurement and so the measurement noise covariance for smart meter measurements is $R^{\mathrm{SM}} \approx 0$. Also,

without measurements of the NW demand in each feeder portion, we cannot quantify the NW demand approximation error.

## IV. Aggregate Models for Energy Disaggregation

We create separate aggregate load models for the $N$ demand components in each feeder portion (i.e., for the elements of $\theta_t$) using multiple linear regressions and historical smart meter and feeder measurements. The regression models predicting the active and reactive demand for load component $l$ on feeder portion $\mathcal{F}_m$, respectively $\widehat{P}_t^{l,m}$ and $\widehat{Q}_t^{l,m}$, are

$$\widehat{P}_t^{l,m} = \beta^{l,m} D_t^l \quad m \in \mathcal{M} \text{ and } l = 1, \ldots, N \tag{17}$$

$$\widehat{Q}_t^{l,m} = \gamma^{l,m} D_t^l \quad m \in \mathcal{M} \text{ and } l = 1, \ldots, N \tag{18}$$

where $\beta^{l,m}$ and $\gamma^{l,m}$ are row vectors of regression parameters for $\mathcal{F}_m$. The input features are defined as $D_t^l \triangleq \left[D_t^{l,\mathrm{CAL}} \;\; D_t^{l,\mathrm{WEA}} \;\; D_t^{l,\mathrm{NW}}\right]^{\mathrm{T}}$, where $D_t^{l,\mathrm{CAL}}$, $D_t^{l,\mathrm{WEA}}$, and $D_t^{l,\mathrm{NW}}$ are row vectors of calendar-based, weather-based, and substation- and network-based features, respectively. To perform the regression, we assume that historical input feature data are available, and that we can compute historical $\theta_t$ measurements/estimates.

## V. Case Studies

We perform case studies with one-minute time-steps to evaluate the performance of the disagregation algorithm and aggregate models using scenarios of real-time measurement availability. The power system entity disaggregates the distribution feeder demand into the aggregate AC demand, the aggregate OL demand, and the NW demand. Note that we do not include distributed generation or storage in the case studies. Section V-A presents the method of generating the ground-truth data of the case studies, i.e., the plant data, which is based on real-world data. Sections V-B and V-C detail the disaggregation algorithm and the models used within the disaggregation algorithm, respectively. Offline model computation and algorithm tuning for the case studies rely on 17 days of historical data, which is not a large amount of data for the input features of the models, e.g., time of day. Sections V-D, V-E, and V-F respectively detail the cases, the performance evaluation, and the results. The case studies illustrate how the availability of heterogeneous real-time measurements influences disaggregation accuracy.

### A. Case Study Plant

The plant consists of a feeder model and load models that incorporate both outdoor temperature and active power demand data from [19]. The feeder model is the 13-node test feeder [20], a three-phase feeder with unbalanced loads; Fig. 4 depicts the single-line feeder diagram, where we have added node 651 to indicate the secondary side of the voltage regulator. We assume that i) all loads are wye-connected; ii) the switch is closed; iii) the line parameters from node 671 to 692 are identical to the line from node 692 to 675; iv) node 680 contains a load of $(290 + j212.0)$, $(170 + j80.0)$, and $(128 + j86.0)$ kW for phases A, B, and C, respectively;

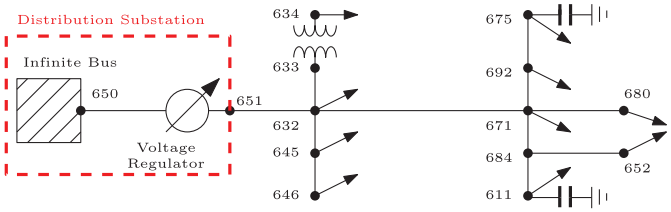


Fig. 4. Single-line diagram of the IEEE 13-node test feeder.

v) the capacitor banks are always connected; and vi) tap changes have a lockout time of five minutes for each phase. To transform specified delta-connected loads to wye-connected loads, we connect the line-to-line loads (X-Y) as line-to-neutral loads (X-N), where X and Y are arbitrary phases and N is neutral. We linearly interpolate the hourly weather data down to one-minute time-steps, the frequency of the demand data. We connect houses to each node and phase by randomly sampling with replacement from the houses in Austin, TX, USA in [19] until the total average active power demand for August 31, 2017 is greater than the corresponding feeder model load. This results in 2,388 houses, each with an AC, connected to the feeder. While we use the loads specified in the test feeder to connect houses to the feeder, the data for each house varies throughout the case studies. Therefore, the realized load will deviate from the specified feeder values, but the average realized load values are near the specified values.

The plant contains models of the AC demand, $P_t^{n,\mathrm{AC}} + jQ_t^{n,\mathrm{AC}}$, connected to each node $n$. The AC demand model is based on the "performance model" from [21], [22], which has a voltage- and temperature-dependent reactive demand component and a temperature-dependent active demand component. The "performance model" was developed for transmission systems, but it is appropriate for this work as we are interested in the aggregate, steady-state AC demand at each node within a distribution network. Each time-step sets the model parameters by first computing $P_t^{n,\mathrm{AC}} = \sum_{j \in \mathcal{J}^{n,\mathrm{AC}}} P_t^{j,\mathrm{AC}}$, where $P_t^{j,\mathrm{AC}}$ is the active power demand data of AC $j$ at time $t$ from [19], and $\mathcal{J}^{n,\mathrm{AC}}$ is the set of ACs connected to node $n$. The data $P_t^{j,\mathrm{AC}}$ is temperature dependent, and the performance model's active demand component is independent of voltage at normal voltage levels [22]. The model's reactive component, which was developed in [21], is

$$Q_t^{n,\mathrm{AC}} = b_1 + \frac{b_2}{(v_t^n - b_0)} + b_3(v_t^n - b_0) + b_4(v_t^n - b_0), \tag{19}$$

where $b_0$, $b_2$, $b_3$, and $b_4$ are parameters that depend on the outdoor temperature, and where $b_1$ is a parameter the depends on $P_t^{n,\mathrm{AC}}$. We compute the parameters offline to resemble the curves of [22, Fig. 16].

The plant also computes the OL demand, $P_t^{n,\mathrm{OL}} + jQ_t^{n,\mathrm{OL}}$, connected to each node $n$ using voltage-dependent polynomial constant impedance (Z), constant current (I), and constant power (P) models, i.e., ZIP models, for the different OL loads within the data. The OL demand at each node is the sum of the demand of the OL loads connected to that node. At each time-step, we set the rated active power demand of each ZIP model to the measured demand from [19] of the load, and

the remaining ZIP model parameters are from [23], [24]. The coffee maker, fan, lighting, microwave, refrigerator, and water heater loads use parameters from [24]. The drier heater, drier tumbler, freezer, heat pump, office equipment, and washing machine loads use parameters from [23]. We assume lighting loads are incandescent, water heaters are resistive heaters, furnaces/heaters are heat pumps, and kitchen plugs containing small appliances correspond to a coffee maker. We sum the remaining OL loads in the data of each house into a miscellaneous ZIP model that uses the "residential stratum F" model parameters from [24].

The simulation computes the complex voltages and complex currents within the feeder using the feeder model and the load models within the backward-forward sweep algorithm [25]. At each time-step in the simulation, the voltages at the feeder nodes are initially assumed to be at their rated values, and the backward-forward sweep algorithm iterates to compute the complex voltages and complex currents. The load models are initialized with the rated voltage and their parameters, and the models update the voltage and resulting demand after each iteration. The backward-forward sweep algorithm converges if the voltage changes less than $1.0\times10^{-6}$ in per-unit voltage at node 671 during an iteration. After convergence, the voltage magnitude is checked at node 671, where the allowable voltage bandwidth is 121-123 V (for a 120 V base), and tap positions change if necessary. If the tap position changes, the backward-forward sweep algorithm is restarted with the new tap positions and the process repeats. If the tap position is unchanged, the simulation advances to the next time-step.

### B. Disaggregation Algorithm Implementation

This subsection details the implementation of the disaggregation algorithm used within the case studies. We define $\theta_t$, select the user-defined functions in (1), and summarize the parameter settings. We define $\theta_t$ using two feeder portions based on nodes 651 and 671 in Fig. 4—$\theta_t = \left[P_{\mathcal{F}_{651}} \;\; P_{\mathcal{F}_{671}} \;\; `Q_{\mathcal{F}_{651}} \;\; Q_{\mathcal{F}_{671}}\right]$—where $P_{\mathcal{F}_{651}}$, $P_{\mathcal{F}_{671}}$, $Q_{\mathcal{F}_{651}}$, $Q_{\mathcal{F}_{671}} \in \mathbb{R}^3$ each contain three demand components—the AC, OL, and NW demand. We consider 650 as the root node, and nodes 651 and 671 are measurement points detailed in Section V-D. We set $D(\theta\|\widehat{\kappa}_t) = \frac{1}{2}\|\widehat{\Pi}_t^{-\frac{1}{2}}(\theta - \widehat{\kappa}_t)\|_2^2$ and $\ell_t(\widehat{\theta}_t, y_t) = \frac{1}{2}\|(\Pi_t^{\mathrm{y}})^{-\frac{1}{2}}(C_t\widehat{\theta}_t - y_t)\|_2^2$. We compute $\widehat{\Pi}_t$ using prediction errors of the disaggregation algorithm aggregate models for simulated data from August 14-30, 2017. The resulting closed form of (1) is

$$\widehat{\kappa}_{t+1} = \widehat{\kappa}_t + \eta^{\mathrm{s}}\widehat{\Pi}_t C_t^T\left(\Pi_t^{\mathrm{y}}\right)^{-1}\left(y_t - C_t\widehat{\theta}_t\right). \tag{20}$$

We apply the algorithm to simulations for August 31, 2017 to tune the parameters within (20). We roughly tune the parameters to minimize the disaggregation error when applied to this training data. Specifically, we incremented $\eta^{\mathrm{s}}$ in steps of 0.05 and ran the algorithm on the training data to determine the setting that resulted in the lowest error. Slight improvements in accuracy could be achieved via more precise tuning, but this should not influence the results trends. We set $\eta^{\mathrm{s}} = 0.5$ when using model set $\mathcal{M}^{\mathrm{nc}}$ and $\eta^{\mathrm{s}} = 0.2$ when using model set $\mathcal{M}^{\mathrm{c}}$, where $\mathcal{M}^{\mathrm{nc}}$ and $\mathcal{M}^{\mathrm{c}}$ are defined in Section V-C. We set the measurement noise covariances $R^{\mathrm{PQ}}$ and $R^{\mathrm{SM}}$ to $\sigma I$, where $I$ is an appropriately-sized identity matrix in each case, and where $\sigma = 1\times10^{-8}$. We compute $R^{\mathrm{VM}}$ and $R^{\mathrm{VA}}$ using historical data from August 14-30, 2017.

TABLE II
CASE STUDY REAL-TIME MEASUREMENT SCENARIO DEFINITIONS

| Scenario | Models | Real-Time Measurements | Purpose |
|---|---|---|---|
| 1 | $\mathcal{M}^{\mathrm{nc}}$ | None | Evaluate the prediction accuracy of $\mathcal{M}^{\mathrm{nc}}$ |
| 2 | $\mathcal{M}^{\mathrm{c}}$ | Substation complex current | Evaluate the prediction accuracy of $\mathcal{M}^{\mathrm{c}}$ |
| 3 | $\mathcal{M}^{\mathrm{nc}}$ | Substation active power | Benchmark these results against those in [13], [14], which use a similar measurement scenario |
| 4 | $\mathcal{M}^{\mathrm{c}}$, $\mathcal{M}^{\mathrm{nc}}$ | Substation apparent power; substation complex current | Evaluate the disaggregation accuracy with reactive power measurements |
| 5 | $\mathcal{M}^{\mathrm{c}}$ | Scenario 4 measurements; voltage phasors at nodes 650 and 671 | Evaluate the disaggregation accuracy with additional voltage phasor measurements. |

### C. Disaggregation Algorithm Aggregate Model Details

We use two sets of aggregate AC, OL, and NW demand models in the disaggregation algorithm. In each set, we compute six models, one model for each of the three demand components in each of the two feeder portions. We compute the regression parameters using historical data obtained by simulating the plant with data from August 14-30, 2017. The first set of models, denoted $\mathcal{M}^{\mathrm{c}}$, includes input features based on substation complex current measurements. The input features are $D_t^{\mathrm{AC}} = \left[x_t^{\mathrm{tod}} \;\; |i_t^0| \;\; \mathrm{real}(i_t^0) \;\; \mathrm{imag}(i_t^0) \;\; T_t^{\mathrm{o}}\right]^{\mathrm{T}}$, $D_t^{\mathrm{NW}} = D_t^{\mathrm{OL}} = \left[x_t^{\mathrm{tod}} \;\; |i_t^0| \;\; \mathrm{real}(i_t^0) \;\; \mathrm{imag}(i_t^0)\right]^{\mathrm{T}}$. The row vector $x_t^{\mathrm{tod}}$ indicates the time of day; $|\cdot|$, $\mathrm{real}(\cdot)$, and $\mathrm{imag}(\cdot)$ are the magnitude, real component, and imaginary component of the argument, respectively; $i_t^0$ is the complex current measurement; and $T_t^{\mathrm{o}}$ is the outdoor temperature. The second set of models, denoted $\mathcal{M}^{\mathrm{nc}}$, excludes current-based input features. The input features are $D_t^{\mathrm{AC}} = \left[x_t^{\mathrm{tod}} \;\; T_t^{\mathrm{o}}\right]^{\mathrm{T}}$ and $D_t^{\mathrm{NW}} = D_t^{\mathrm{OL}} = x_t^{\mathrm{tod}}$.

### D. Case Definitions

We define cases using five scenarios of real-time measurement availability, real-time smart meter measurement availability, and the model set used within the algorithm. Table II defines the real-time measurement availability scenarios and the applicable model sets. Note that we used the phasor measurement points in Scenario 5 to construct $\theta_t$ in Section V-B. We assume that 1) measurements available in real-time are also available historically, and 2) historical substation demand and smart meter apparent power measurements are always available, which allows computation of $\mathcal{M}^{\mathrm{nc}}$ in any scenario. If real-time smart meter measurements are available, we add a measurement scenario suffix indicating the minutes between their availability For example, scenario 3-30 indicates scenario 3 with real-time smart meter measurements every 30 minutes.

### E. Performance Evaluation

To evaluate disaggregation algorithm performance, we apply the algorithm while simulating the plant using data from

TABLE III
DEMAND COMPONENT RMSE (KW/KVAR/KVA) IN DIFFERENT CASES

| Scenario | Models | Demand Component | | | | | | | | |
|---|---|---|---|---|---|---|---|---|---|---|
| | | AC-P | AC-Q | AC-S | OL-P | OL-Q | OL-S | NW-P | NW-Q | NW-S |
| 1 | $\mathcal{M}^{\text{nc}}$ | 181.4 | 45.4 | 187.0 | 179.2 | 52.7 | 186.8 | 50.0 | 157.0 | 165.4 |
| 2 | $\mathcal{M}^{\text{c}}$ | 64.1 | 16.0 | 66.1 | 68.0 | 20.0 | 70.9 | 5.6 | 8.2 | 9.9 |
| 3 | $\mathcal{M}^{\text{nc}}$ | 129.6 | - | - | 114.0 | - | - | 23.0 | - | - |
| 3-60 | $\mathcal{M}^{\text{nc}}$ | 77.5 | - | - | 63.0 | - | - | 16.8 | - | - |
| 3-30 | $\mathcal{M}^{\text{nc}}$ | 69.6 | - | - | 55.7 | - | - | 13.8 | - | - |
| 3-15 | $\mathcal{M}^{\text{nc}}$ | 61.1 | - | - | 47.0 | - | - | 10.9 | - | - |
| 4 | $\mathcal{M}^{\text{nc}}$ | 103.5 | 25.9 | 106.7 | 97.0 | 33.1 | 102.5 | 8.7 | 21.4 | 23.1 |
| 4 | $\mathcal{M}^{\text{c}}$ | 64.1 | 16.0 | 66.1 | 64.8 | 19.6 | 67.7 | 5.7 | 8.2 | 10.0 |
| 4-60 | $\mathcal{M}^{\text{c}}$ | 46.9 | 11.7 | 48.3 | 48.7 | 15.6 | 51.1 | 5.6 | 7.7 | 9.5 |
| 4-30 | $\mathcal{M}^{\text{c}}$ | 45.7 | 11.4 | 47.1 | 47.5 | 14.9 | 49.8 | 5.2 | 7.1 | 8.8 |
| 4-15 | $\mathcal{M}^{\text{c}}$ | 41.2 | 10.3 | 42.4 | 43.1 | 13.4 | 45.2 | 5.0 | 6.4 | 8.1 |
| 5 | $\mathcal{M}^{\text{c}}$ | 61.7 | 15.4 | 63.6 | 62.2 | 20.2 | 65.4 | 6.1 | 13.6 | 15.1 |

September 1-4, 2017. The RMS error (RMSE) of the estimated AC, OL, and NW demand quantifies the performance. The RMSE for complex-valued predictions/estimates $\widehat{\psi}_t$ and the true values $\psi_t$ over $N^{\text{ts}} = 4321$ time-steps is RMSE $= \sqrt{\sum_{t=1}^{N^{\text{ts}}} |\psi_t - \widehat{\psi}_t|^2 / N^{\text{ts}}}$. We evaluate the disaggregation accuracy at the feeder head, and so the disaggregation error over the entire feeder is $\psi_t - \widehat{\psi}_t = \sum_{m \in \mathcal{M}} (\psi_t^m - \widehat{\psi}_t^m)$ for $m \in \mathcal{M}$.

### F. Results

Table III summarizes the RMSEs averaged over the three phases for the demand components. The "Models" column indicates the model set used. The AC-P, AC-Q, and AC-S entries correspond to the active, reactive, and apparent power of the AC demand; the OL and NW demand have similar entries. We exclude -Q and -S entries in Scenario 3 and its variants as the disaggregation algorithm does not include reactive power in these cases. Figure 5 depicts time series of the realized demand component magnitudes for phase A along with their predictions in Scenarios 1 and 2. The execution time for the algorithm was 0.0025 seconds per time-step on average.

We evaluate the impact of real-time substation current measurements on prediction accuracy by comparing Scenarios 1 and 2, which use $\mathcal{M}^{\text{nc}}$ and $\mathcal{M}^{\text{c}}$, respectively. Average RMSEs across the three demand components for Scenario 2 are 73.1% lower than Scenario 1. The RMSEs of AC-P, OL-P, and NW-P are respectively reduced by 64.7%, 62.1%, and 88.8%. Figure 5 depicts these accuracy improvements. These results indicate that real-time substation current measurements can significantly improve the prediction accuracy of the aggregate models used within the disaggregation algorithm.

We evaluate the impact of substation reactive power measurements by comparing Scenarios 3 and 4 using $\mathcal{M}^{\text{nc}}$. RMSEs of AC-P, OL-P, and NW-P decrease from Scenario 3 to 4 by 20.1%, 14.9%, 62.2%, respectively. These results indicate that substation reactive power measurements can significantly improve disaggregation accuracy, which [10] also found.

We evaluate the impact of real-time smart meter measurements at increasing frequencies by comparing i) Scenarios 3, 3-60, 3-30, and 3-15 and ii) Scenarios 4 using $\mathcal{M}^{\text{c}}$, 4-60, 4-30, and 4-15. RMSEs averaged across AC-P, OL-P, and NW-P decrease 37.3%, 45.8%, and 54.7% from Scenario 3 to 3-60, 3-30, and 3-15, respectively. Average RMSEs across all demand components decrease 18.1%, 21.9% and 28.8% from Scenario 4 to 4-60, 4-30, and 4-15, respectively. These results indicate that disaggregation accuracy improves as real-time smart meter measurements are available more frequently.

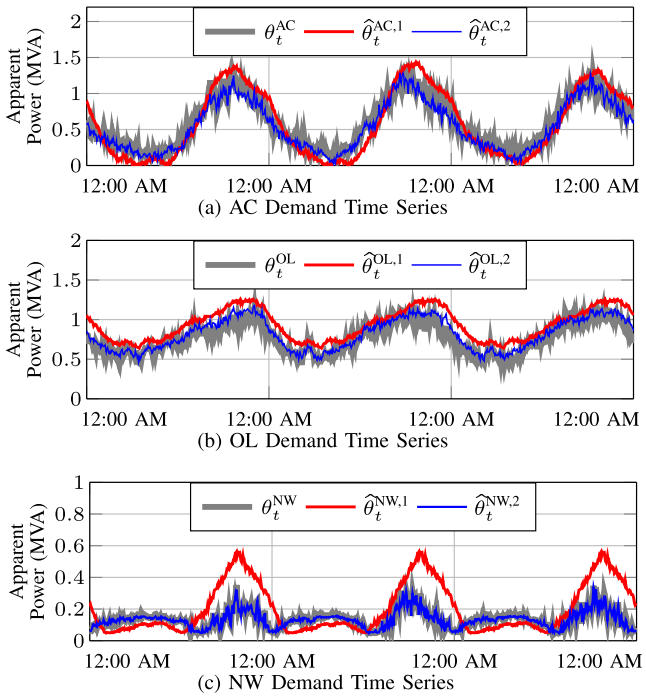


Fig. 5. Time series of the realized demand magnitudes for phase A and the Scenario 1 and 2 predictions. The superscripts denote the scenarios.

We evaluate the impact of real-time voltage phasor measurements by comparing Scenarios 4 and 5. The RMSE decreases 3.7% and 4.0% from Scenario 4 to 5 for AC-P and OL-P, respectively, while the RMSE for NW-P increases 7.0%. These results indicate that voltage phasor measurements may be beneficial, but more accurate output matrices, excluding capacitor bank power injections from the NW demand, and better NW demand estimates for feeder portions may make the measurements more useful.

Note that [13], [14] include case studies to explore the impact of model accuracy, parameter tuning, and the choice of functions used in the disaggregation algorithm for measurement Scenario 3, where the only available measurement is the active power at the feeder head. We do not present additional case studies exploring these impacts in this work, as the results for the various scenarios follow similar trends as in these prior case studies.

## VI. CONCLUSION

This work developed an energy disaggregation algorithm to separate the measured, real-time demand of a distribution feeder into $N$ components, where one component consisted of the network losses and capacitor bank power injections. The algorithm used a modified version of DMD with sensor fusion to allow measurements from multiple sources on different timescales to be used within the algorithm.

Output matrices were developed to allow fusion of active and reactive power flows, differences in squared bus voltage magnitudes, differences in bus voltage angles, and smart meter measurements. Aggregate models were also developed that utilize real-time substation current measurements. Case studies sought to disaggregate the real-time feeder demand into the AC demand, the OL demand, and the NW demand within a plant consisting of a three-phase, unbalanced distribution feeder.

Results indicated that 1) incorporating real-time substation measurements into the disaggregation algorithm aggregate models can significantly improve the models' prediction accuracy, 2) real-time substation reactive power measurements can improve disaggregation accuracy, 3) real-time smart meter measurements at higher frequencies increasingly improves the energy disaggreation algorithm's accuracy, and 4) measurements of the complex voltage at points within the feeder and at the substation can further improve accuracy.

The disaggregation algorithm is highly scalable. In real-time, it requires evaluating the models, rather than optimizing over the models, and therefore relies on simple computations, e.g., matrix/vector multiplication. The size of these computations increases with the number of available measurement locations and the number of demand components being disaggregated. The algorithm can run in parallel on separate feeders, which limits the size of the problem. To obtain individual appliance measurements/estimates requires submetering or household energy disaggregation on smart meter data, where the latter could be computationally heavy. However, again, parallel processing can be used as needed.

Furthermore, the type of data available to the aggregator depends on its affiliation, i.e., whether it is part of the utility or is a third-party aggregator. Closer ties to the utility would result in greater access to measurements and capabilities of the disaggregation algorithm. However, if all of the data is not available to the aggregator, the flexibility of the algorithm allows it to incorporate whatever information is available.

Future work should 1) incorporate delta-connected loads; 2) include estimated/identified resistances and reactances; 3) determine whether capacitor bank switching can be detected and removed from the NW demand; 4) investigate methods to better approximate the losses in feeder portions using line lengths and possibly line parameters; 5) modify the algorithm to make it applicable to meshed networks; 6) incorporate distributed generation; 7) simultaneously disaggregate demand responsive load, distributed generation, and energy storage; and 8) perform disaggregation while sending external control signals to resources.

## REFERENCES


[1] "Distributed energy resources: Technical considerations for the bulk power system," Federal Energy Regul. Comm., Washington, DC, USA, Rep. AD18–10-000, Feb. 2018. [Online]. Available: https://www.ferc.gov/CalendarFiles/20180215112833-der-report.pdf

[2] B. Foster *et al.*, "Assessment of demand response & advanced metering," FERC, Washington, DC, USA, Rep., Dec. 2017. [Online]. Available: https://www.ferc.gov/legal/staff-reports/2017/DR-AM-Report2017.pdf

[3] D. Atanackovic and V. Dabic, "Deployment of real-time state estimator and load flow in BC Hydro DMS—Challenges and opportunities," in *Proc. IEEE Power Energy Soc. Gen. Meeting (PESGM)*, 2013.

[4] A. von Meier, D. Culler, A. McEachern, and R. Arghandeh, "Micro-synchrophasors for distribution systems," in *Proc. IEEE Innovat. Smart Grid Technol. Conf. (ISGT)*, 2014, pp. 1–5.

[5] K. C. Armel, A. Gupta, G. Shrimali, and A. Albert, "Is disaggregation the holy grail of energy efficiency? The case of electricity," *Energy Policy*, vol. 52, pp. 213–234, Jan. 2013.

[6] E. C. Kara, C. M. Roberts, M. Tabone, L. Alvarez, D. S. Callaway, and E. M. Stewart, "Disaggregating solar generation from feeder-level measurements," *Sustain. Energy Grids Netw.*, vol. 13, pp. 112–121, Mar. 2018.

[7] E. C. Kara, Z. Kolter, M. Berges, B. Krogh, G. Hug, and T. Yuksel, "A moving horizon state estimator in the control of thermostatically controlled loads for demand response," in *Proc. IEEE Int. Conf. Smart Grid Commun. (SmartGridComm)*, Vancouver, BC, Canada, 2013, pp. 253–258.

[8] S. E. Z. Soudjani and A. Abate, "Aggregation and control of populations of thermostatically controlled loads by formal abstractions," *IEEE Trans. Control Syst. Technol.*, vol. 63, no. 3, pp. 975–990, May 2014.

[9] Q. Gan and C. J. Harris, "Comparison of two measurement fusion methods for Kalman-filter-based multisensor data fusion," *IEEE Trans. Aerosp. Electron. Syst.*, vol. 37, no. 1, pp. 273–279, Jan. 2001.

[10] Y. Xu and J. V. Milanović, "Artificial-intelligence-based methodology for load disaggregation at bulk supply point," *IEEE Trans. Power Syst.*, vol. 30, no. 2, pp. 795–803, Mar. 2015.

[11] D. Chakravorty, B. Chaudhuri, and S. Y. R. Hui, "Estimation of aggregate reserve with point-of-load voltage control," *IEEE Trans. Smart Grid*, vol. 9, no. 5, pp. 4649–4658, Sep. 2018.

[12] M. Domanovic, G. Dobric, and N. Rajakovic, "Direct method for estimation of demand composition at supply point," in *Proc. IET Mediterr. Conf. Power Gen. Transm. Distr. Energy Convers. (MedPower)*, 2016.

[13] G. S. Ledva, L. Balzano, and J. L. Mathieu, "Real-time energy disaggregation of a distribution feeder's demand using online learning," *IEEE Trans. Power Syst.*, vol. 33, no. 4, pp. 4730–4740, Sep. 2018.

[14] G. S. Ledva, Z. Du, L. Balzano, and J. L. Mathieu, "Disaggregating load by type from distribution system measurements in real time," in *Energy Markets and Responsive Grids*, S. Meyn, T. Samad, I. Hiskens, and J. Stoustrup, Eds. New York, NY, USA: Springer, 2018, pp. 413–437.

[15] E. C. Hall and R. M. Willett, "Online convex optimization in dynamic environments," *IEEE J. Sel. Topics Signal Process.*, vol. 9, no. 4, pp. 647–662, Jun. 2015.

[16] S. Bolognani, N. Bof, D. Michelotti, R. Muraro, and L. Schenato, "Identification of power distribution network topology via voltage correlation analysis," in *Proc. IEEE Conf. Decis. Control (CDC)*, 2013, pp. 1659–1664.

[17] M. E. Baran and F. F. Wu, "Network reconfiguration in distribution systems for loss reduction and load balancing," *IEEE Trans. Power Del.*, vol. 4, no. 2, pp. 1401–1407, Apr. 1989.

[18] R. Dobbe, D. Arnold, S. Liu, D. Callaway, and C. Tomlin, "Real-time distribution grid state estimation with limited sensors and load forecasting," in *Proc. IEEE Int. Conf. Cyber Phys. Syst. (ICCPS)*, 2016, pp. 1–10.

[19] Pecan Street Inc., (2018). *Dataport*. [Online]. Available: https://dataport.cloud/

[20] W. H. Kersting, "Radial distribution test feeders," in *Proc. IEEE Power Eng. Soc. Winter Meeting*, vol. 2, 2001, pp. 908–912.

[21] R. Bravo *et al.*, "Final project report load modeling transmission research," Lawrence Berkeley Nat. Lab., Berkeley, CA, USA, Rep. CEC-500–2013-118, Aug. 2008.

[22] "Dynamic load modeling technical reference document," North Amer. Electric Rel. Corp., Atlanta, GA, USA, Rep., Dec. 2016.

[23] L. M. Hajagos and B. Danai, "Laboratory measurements and models of modern loads and their effect on voltage stability studies," *IEEE Trans. Power Syst.*, vol. 13, no. 2, pp. 584–592, May 1998.

[24] A. Bokhari *et al.*, "Experimental determination of the ZIP coefficients for modern residential, commercial, and industrial loads," *IEEE Trans. Power Del.*, vol. 29, no. 3, pp. 1372–1381, Jun. 2014.

[25] W. H. Kersting, *Distribution System Modeling and Analysis*. Boca Raton, FL, USA, CRC Press, 2012.

**Gregory S. Ledva** (Member, IEEE) received the B.S. degree in mechanical engineering from the Pennsylvania State University, State College, PA, USA, in 2010, the M.S. degree in energy science and technology from ETH Zürich (Swiss Federal Institute of Technology) in 2014, and the Ph.D. degree in electrical engineering: systems from the University of Michigan, Ann Arbor, MI, USA, in 2019, where he is currently a Postdoctoral Researcher. His research interests include modeling, estimation, control, and optimization of distributed energy resources as well as the adaptation of machine learning algorithms for control applications.

**Johanna L. Mathieu** (Senior Member, IEEE) received the B.S. degree in ocean engineering from the Massachusetts Institute of Technology, Cambridge, MA, USA, in 2004, and the M.S. and Ph.D. degrees in mechanical engineering from the University of California, Berkeley, CA, USA, in 2008 and 2012, respectively. She was a Postdoctoral Researcher with the Swiss Federal Institute of Technology (ETH) Zürich, Switzerland. She is an Assistant Professor with the Department of Electrical Engineering and Computer Science, University of Michigan, Ann Arbor, MI, USA. Her research interests include modeling, estimation, control, and optimization of distributed energy resources.